Schweizerischer Erdbebendienst
Service Sismologique Suisse
Servizio Sismico Svizzero
Swiss Seismological Service

ETH
Eidgenössische Technische Hochschule Zürich
Swiss Federal Institute of Technology Zurich

SITE CHARACTERIZATION REPORT

SSMS: Saint-Maurice Hôpital (VS)

Dario Chieppa, Vincent Perron, Donat Fäh

Last Modification: 21th June, 2022

Schweizerischer Erdbebendienst (SED)
Service Sismologique Suisse
Servizio Sismico Svizzero
Servizi da Terratrembels Svizzer
ETH Zürich
Sonneggstrasse 5
8092 Zürich
Schweiz
dario.chieppa@sed.ethz.ch

Contents

Summary

Saint-Maurice (VS) is a village located in southern Switzerland, in Canton Valais. The place was chosen as site for the installation of a new station, called SSMS, as part of the renewal project of the Swiss Strong Motion Network (SSMNet). In order to better assess the local subsurface, we performed a passive seismic array south-west of the seismic station SSMS.

The results of the horizontal-to-vertical spectral ratio (H/V) show a generally homogeneous subsurface characterized by a fundamental peak between 0.39 and 0.41 Hz, a descending flank going down to a trough at about 1.8 Hz and a second H/V peak between 4.87 and 7.74 Hz.

The inversion of the passive seismic array data is performed using *dinver* and Neopsy techniques and allow the estimation of the velocity profiles down to 750 m. All velocity profiles show similar features in the first 30 meters with two shallow layers with thickness of 3 and 14 m, respectively. A third layer of about 7-8 m thickness shows a strong velocity contrast (V_s = 2100 m/s) and it is followed by a velocity inversion underneath, starting at about 24 m. At about 100 m, a similar interface can be seen by most of the velocity profiles, with the exception of Neopsy Maximum Likelihood model, with S-wave velocities between 703 and 1019 m/s. At higher depths, the inverted velocity profiles present different behaviors and depths for the half-space. For most of the velocity profiles (*SSMS7l*, *SSMS9l*, *SSMS13l* and *SSMS fix*), the half-space is located between 695 and 750 meters and has S-wave velocities between 1460 and 2008 m/s.

The V_{S30} value of the site is 495.1 m/s, corresponding to soil class B in EC8 and C in SIA261 classifications. The theoretical shear-wave transfer functions from the retrieved V_S profiles predicts an amplification function between 0.2 and 30 Hz with amplitudes ranging from 0.66 to 5.40. The amplification function has amplitudes which are comparable with the amplitude of the empirical amplification function recorded at seismic station SSMS in the frequency range 2-30 Hz and shape which is in disagreement.

1 Introduction

The station SSMS is part of the Swiss Strong Motion Network (SSMNet). The station was installed on 20 May 2021 in the framework of the second phase of the Swiss Strong Motion Network (SSMNet) renewal project (Fig. 1). In order to better characterize the underground, to estimate the fundamental frequency of the site and the shear wave velocity, a passive array measurement was carried out on 27 September 2021.

The site is of interest for its location in a populated area in southern Switzerland, for the possibility to improve the network coverage of canton Valais, an area with medium seismicity, and its proximity to the hospital of Saint-Maurice. From a geological point of view, the study area is located on river gravel deposits (Holocene) changing towards west into limestones and marlstones of the autochtone and parautochtone Mesozoic units.

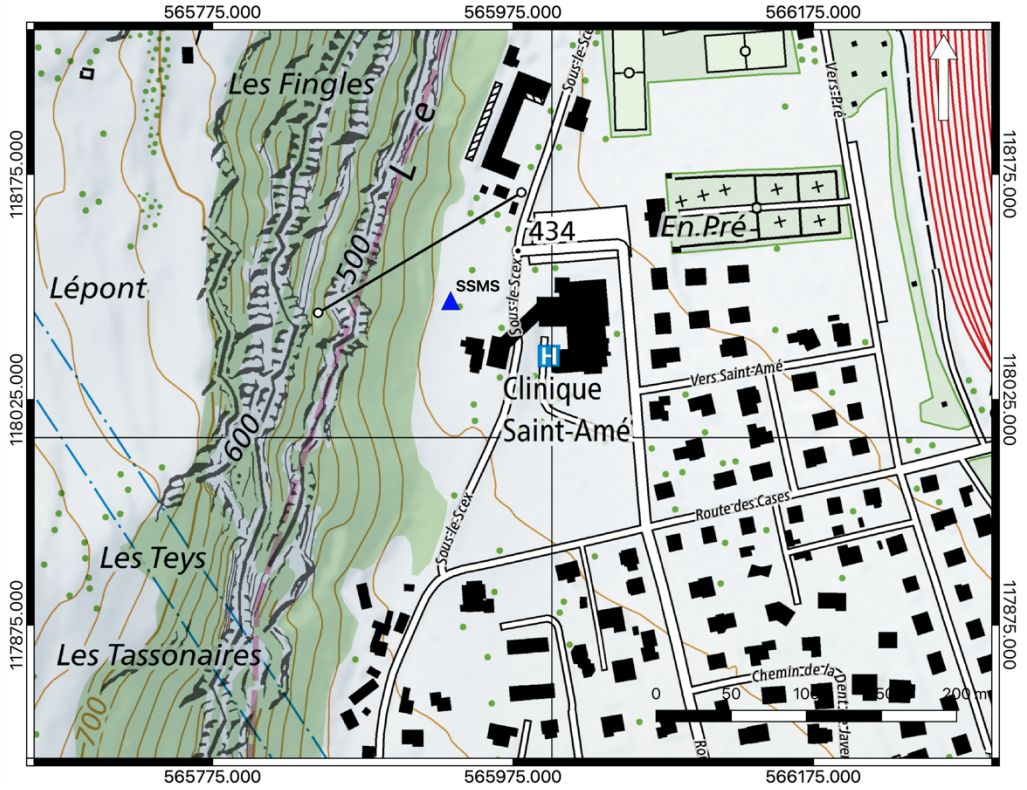

Figure 1: Map showing the location of the strong motion station (blue triangle) in Saint-Maurice. Source: Federal Office of Topography.

2 Geological setting

A geological map of the surroundings south-west of Saint-Maurice city center is shown in Fig. 2. Red dots represent the locations of the passive array, the blue triangle the location of the SSMS station. Thirteen sensors are located on river gravels of Holocene age (light gray), while the remaining three stations and the seismic station SSMS are installed on fine-grained scree of Holocene age (white with blue dots). Towards west, the cliff is made of sandstone, limestone and marlstone changing into siliceous limestone, Echinoderms limestone and marlstone (lower Cretaceous age). These lithologies are shown in green and ochre colors, respectively.

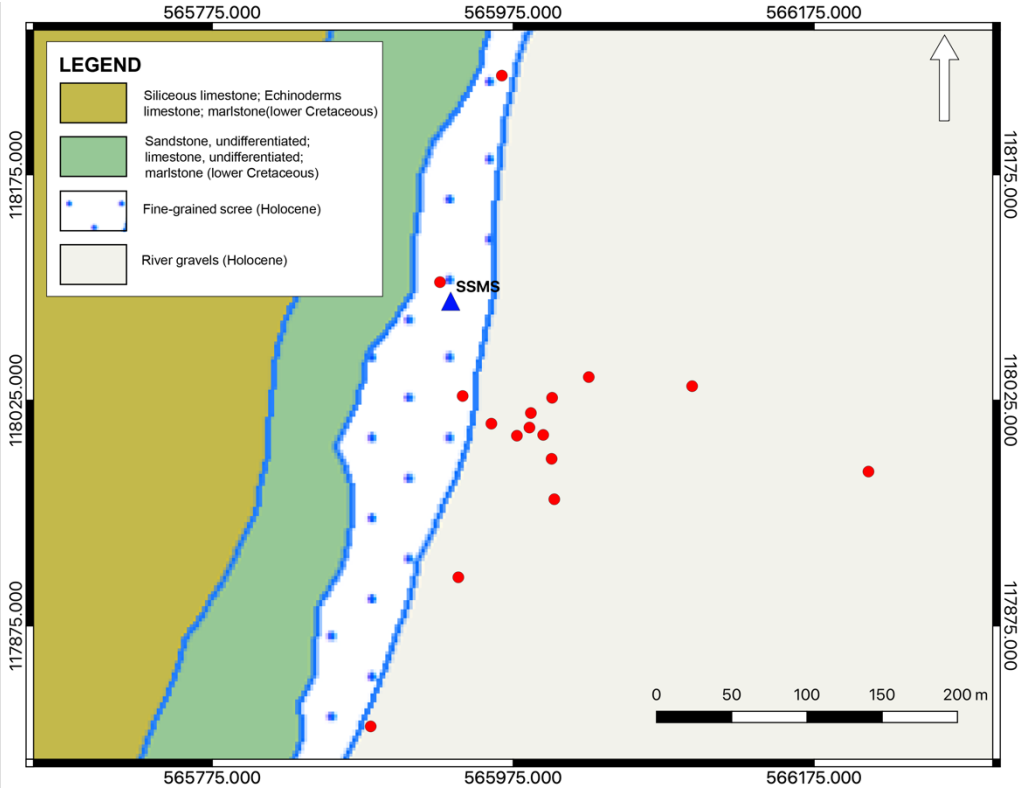

Figure 2: Geological map of the Saint-Maurice area. The stations of the passive array recordings are indicated by red dots, whereas the position of the strong-motion station SSMS is shown by a blue triangle. Source: Federal Office of Topography.

3 Passive site characterization measurements

3.1 Data set

To characterize the deep underground structure around the seismic station, a passive seismic measurement was performed in September 2021 by deploying a single array of 16 stations (Fig. 4). The stations were planned to be located on five rings of different radii around a central station. The three stations of each ring were planned to be rotated 120 degrees one from the other and have radii of 10, 25, 50, 110 and 230 meters. The array central station (SSMS69) is located 90 m south-east from the seismic station SSMS. Each ring, starting from the second, is rotated with respect to the inner ring of 20, 20, 25 and 23 degrees.

Each installation consisted of a Lennartz 5s sensor connected to a Centaur digitizer, with the exception of four stations in the central part which had two sensors connected to the same digitizer. The station names are composed of "SSMS" followed by a two-digit number between 42 and 49, 52 and 55, 62, 63, 69 and 74 (corresponding to the Centaur digitizer serial number for numbers lower than 60 plus 20 to distinguish the use of the second channel). The array recording time was 183 minutes (10980 s). The station locations were measured by a differential GPS system (Leica Viva GS10) which was set up to measure with a precision better than 5 cm. Unfortunately, due to several trees in the center of the array, the precision goes up to 47 cm.

Figure 3: Seismic station installation example for the measurements in Saint-Maurice.

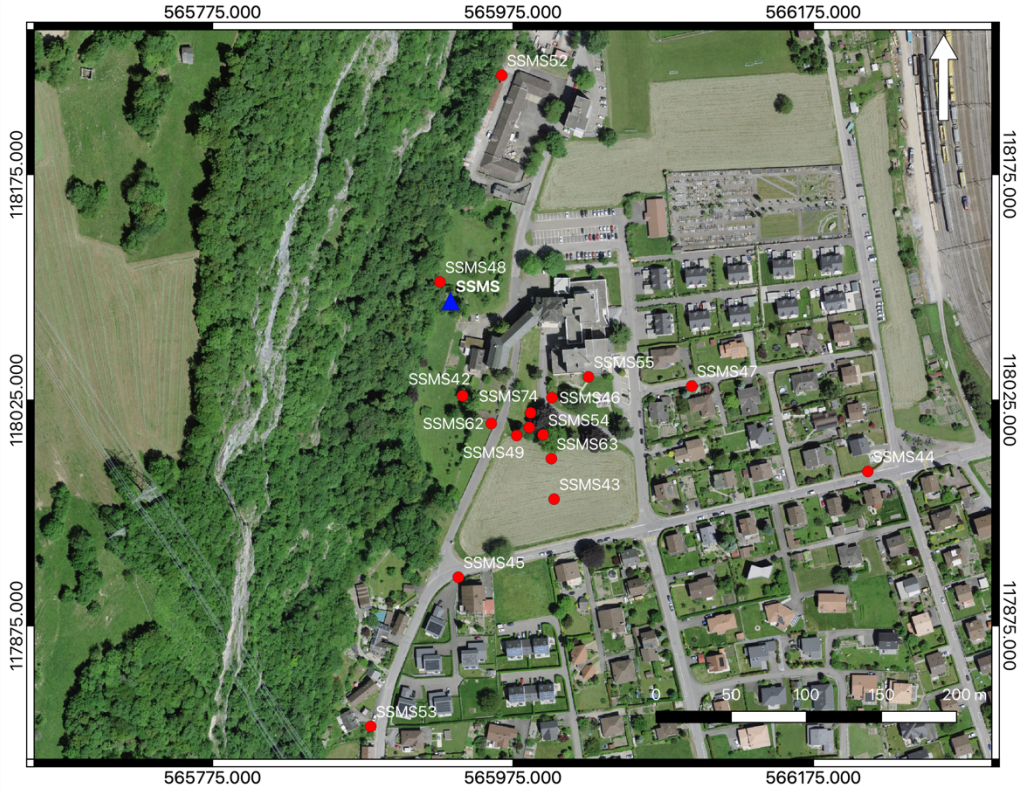

Figure 4: Layout of the array measurement in Saint-Maurice. The locations of the stations for the passive seismic measurement are indicated by the red dots. The blue triangle indicates the seismic station site. Source: Federal Office of Topography.

3.2 H/V and RayDec ellipticity curves

Figure 5 shows the H/V curves (left) determined using Geopsy software (Wathelet et al. 2020) and the ellipticity curves (right) computed using the RayDec technique (Hobiger et al., 2009) for all stations of the passive array.

Most of the H/V curves show similar trends at low and high frequencies, meaning that the underground below the study area is rather homogeneous. The H/V curves show an asymmetric peak at about 0.4 Hz followed by a trough at 0.55 Hz. To the right of the trough, the amplitude of the H/V curves decreases to a minimum of 0.38 at 1.8 Hz and show a narrow trough at several sites. At other sites, instead, the trough in the H/V curves is wider and shifted at higher amplitudes. A second H/V peak is recognized at many sites between 4.87 and 7.74 Hz. Due to the local variability of the shallowest underground, the H/V curves show some variability at high frequencies. A third peak located at 0.71 Hz was also recognized at two sites in the center of the array: SSMS43 and SSMS54. The peak was distinguished by the shape of the H/V curves and it was picked using the Fourier spectrum computed for the vertical component.

Fig. 6 shows the lateral variability of the two peaks observed in the H/V curves. The third peak (green crosses in Fig. 5), picked only at two sites, is not shown here. The map on the left shows the peak at low frequency, while the one on the right reports the frequencies of the second H/V peak at higher frequencies. The first peak can be seen only at the center of the study area and show values over a narrow frequency range; the second peak has homogenous values in the center of the

array changing, in frequency, when moving towards the outer rings. The outermost points towards south and east show the lowest values for the H/V peak at 5.34 and 4.87 Hz, respectively.
The RayDec technique (Hobiger et al., 2009) is meant to eliminate the contributions of other wave types than Rayleigh waves and give a better estimate of the ellipticity. The RayDec ellipticity curves for all stations of the array show a pattern similar to the curves obtained with the H/V analysis. The peak at low frequency is not well defined as for the H/V curves, with the exception of station SSMS69 (dark green curve), while the trough and the subsequent peak at higher frequency are pretty clear for most of the curves. High variability exists at high frequencies above 7 Hz, as for the H/V curves. At low frequency, two ellipticity curves for the seismic stations SSMS48 and SSMS43 show much higher amplitudes and completely different shapes. The dark green curve in Fig. 5 (right plot) indicates the array central station (SSMS69), while the red curve shows the RayDec ellipticity for the SSMS48 station located close to SSMS station.

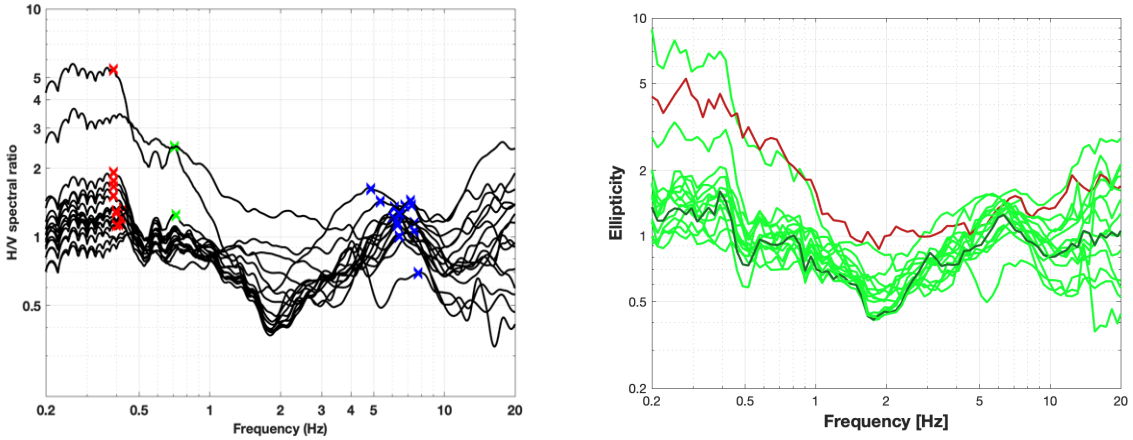

Figure 5: Left: H/V curves of the different stations of the array measurement in Saint-Maurice with picked fundamental frequency (red cross) and first higher mode (blue cross). At two sites, a third peak is shown by a green cross. Right: RayDec ellipticities for all stations of the array. The curve of SSMS69, the array center, is highlighted in dark green, whereas the curve SSMS48, linked to the measurement nearby the station is highlighted in dark red.

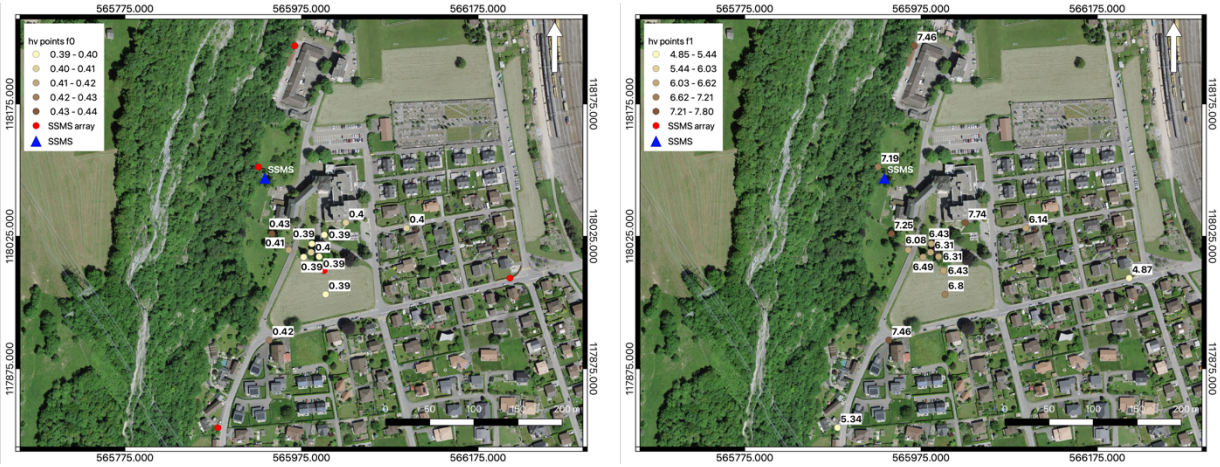

Figure 6: Map showing the variation in frequency for the H/V fundamental (left) and first higher (right) peaks over the area of Saint-Maurice. Source: Federal Office of Topography.

3.3 Polarization measurements

The polarization analysis was performed according to Burjánek et al. (2010) and Burjánek et al. (2012). The results for SSMS69, the array center, and SSMS48, the closest station to the SSMS station are shown in Fig. 7. The two sites show the variability of the underground between the center of the array and the western sector where SSMS station is located. At the sites located in the center of the array, in the southern and in the eastern sectors the ground motion is quasi-linear polarized (0.2) from the H/V peak (at about 0.45 Hz) to 1 Hz. Towards higher frequencies, the ground motion becomes elliptical (0.4) and remain such as till 30 Hz (Fig. 7 – left plot, top row). At SSMS48, the ground motion changes from linear at low frequency (up to 0.4 Hz), to quasi-linear at about 1.8 Hz and then elliptical above 5 Hz (Fig. 7 – left plot, bottom row).
The ground motion at low frequency is inclined between 10 and 40 degrees at all sites; this effect is probably due to the 100 meters cliff located west of the deployed array.
There is no predominant direction of polarization but several weak east-west and north-west south-east directions can be distinguished (Fig. 7 – right plot bottom line).

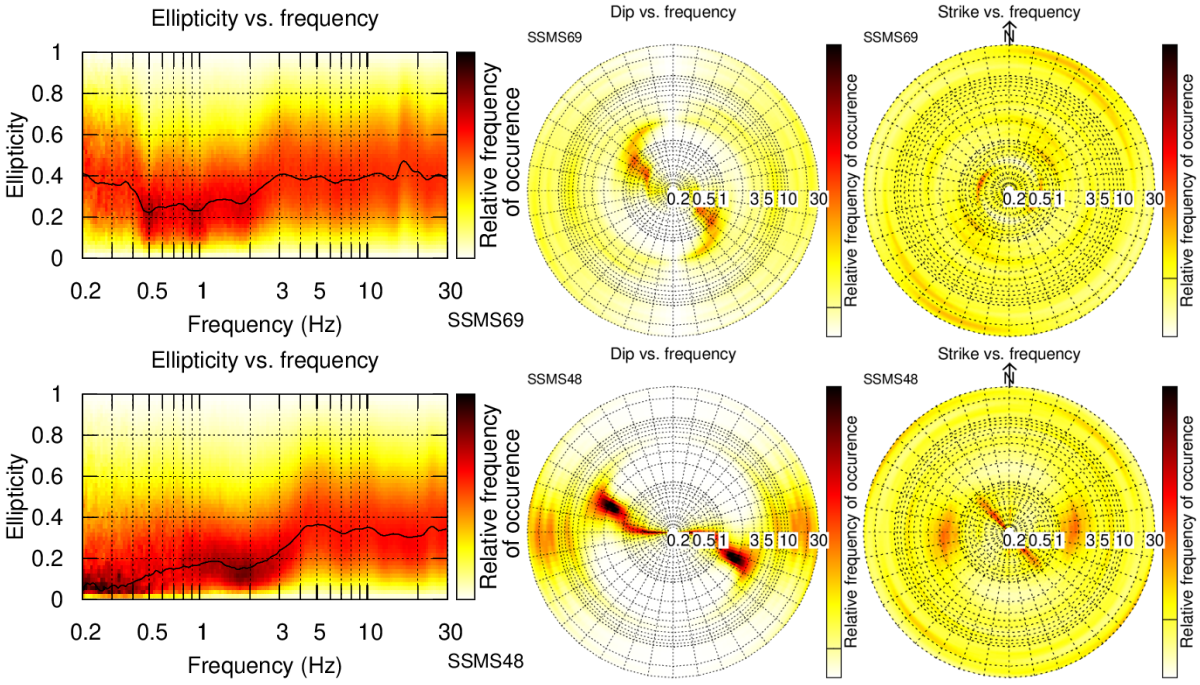

Figure 7: Polarization analysis of station SSMS69 (top) and SSMS48 (bottom).

3.4 3-component high-resolution FK

The results of the 3-component high-resolution FK analysis (Poggi and Fäh, 2010) are shown in Figs. 8 and 9. For Love waves, using the transverse component, two dispersion curves were picked between 1.47 and 15.06 Hz, the one at lower velocities, and between 8.35 and 20.64 Hz, the other. Four dispersion curves were picked for the Rayleigh waves using the vertical (2) and the radial (2) components. For the vertical component the first curve was picked between 1.08 and 16.30 Hz; it shows a descending trend, an almost flat portion (between 2 and 10 Hz) and a gently dipping

portion. The second curve for the vertical component was picked between 5.41 and 16.30 Hz and presents a straight trend with seismic velocities decreasing at higher frequencies. The two curves for the radial component stretch between 1.54 and 22.33 Hz and between 2.88 and 14.48 Hz. The curve at low velocity is discontinuous and shows a flat portion up to 7 Hz followed by a descending trend up to 20 Hz; the other curve shows a straight trend over the entire frequency range. Over the same frequency range as the dispersion curves picked for the vertical and radial components, the ellipticity curves are picked (Fig. 9). The curves in the left column of Fig. 9 correspond to the curves at low velocity for the vertical and radial components, top and bottom respectively, while the right column shows the two curves at higher velocity for the same components. The top curves for the vertical component show a trough-peak-trough sequence and a trough only; the other two curves (bottom row) are mostly flat and show a mild trough at about 10 Hz.

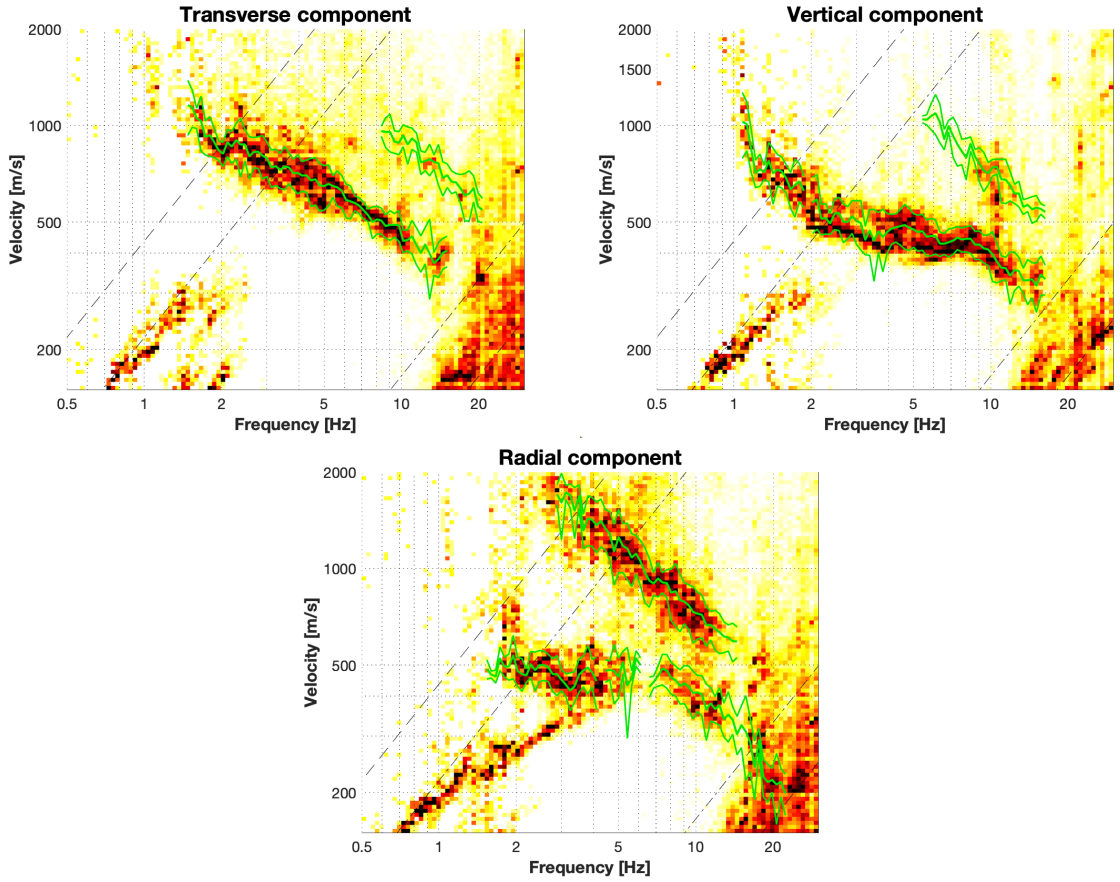

Figure 8: Dispersion curves for the transverse (top left), vertical (top right) and radial (bottom) components obtained with the 3-component HRFK algorithm (Poggi and Fäh, 2010). The dashed and dotted black lines are the array resolution limits. The solid and dashed green lines represent the data picking (central line) and the standard deviation (outer lines).

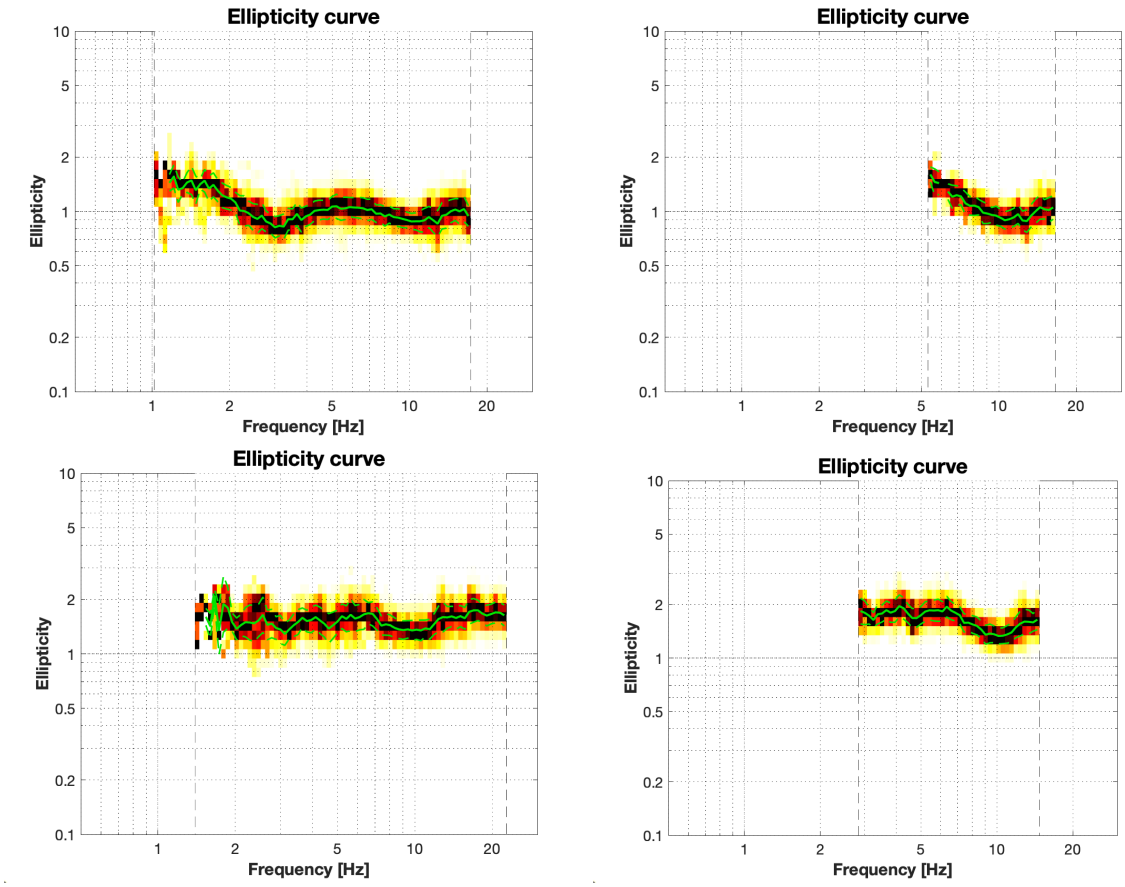

Figure 9: Ellipticity curves for the vertical (top row) and radial (bottom row) components using the 3-component HRFK algorithm (Poggi and Fäh, 2010). Left column shows the mode picked at lower velocity, while the right column the mode at higher velocities. The dashed vertical lines represent the lower and upper frequencies for the picked dispersion curves. The solid and dashed green lines represent the data picking (central line) and the standard deviation (outer lines).

3.5 WaveDec

The results of WaveDec technique (Maranò et al., 2012) are shown in Fig. 10. This technique estimates the properties of single or multiple waves simultaneously with a maximum likelihood approach. In order to get good results, the parameter γ must be tuned to modify the sharpness of the wave property estimation between purely maximum likelihood estimation and a Bayesian Information Criterion. Here, a value of $\gamma = 0.5$ was used, corresponding to an equal mix of maximum likelihood algorithm and Bayesian Information Criterion estimation.

The picking of dispersion curves in WaveDec is performed in the wavenumber-frequency domain but it is here shown in the velocity-frequency domain (Fig. 10). The Love wave dispersion curve was continuously picked between 1.15 and 12.80 Hz (top left plot); the Rayleigh wave dispersion curve was picked between 1.29 and 13.53 Hz (top right plot). The ellipticity angle curve for the picked Rayleigh wave dispersion curve has negative values slightly below zero at 1.43 Hz and

stabilize at about -pi/4 between 3.65 and 13.53 Hz. The particle motion for the picked dispersion curve is retrograde over the entire frequency range.

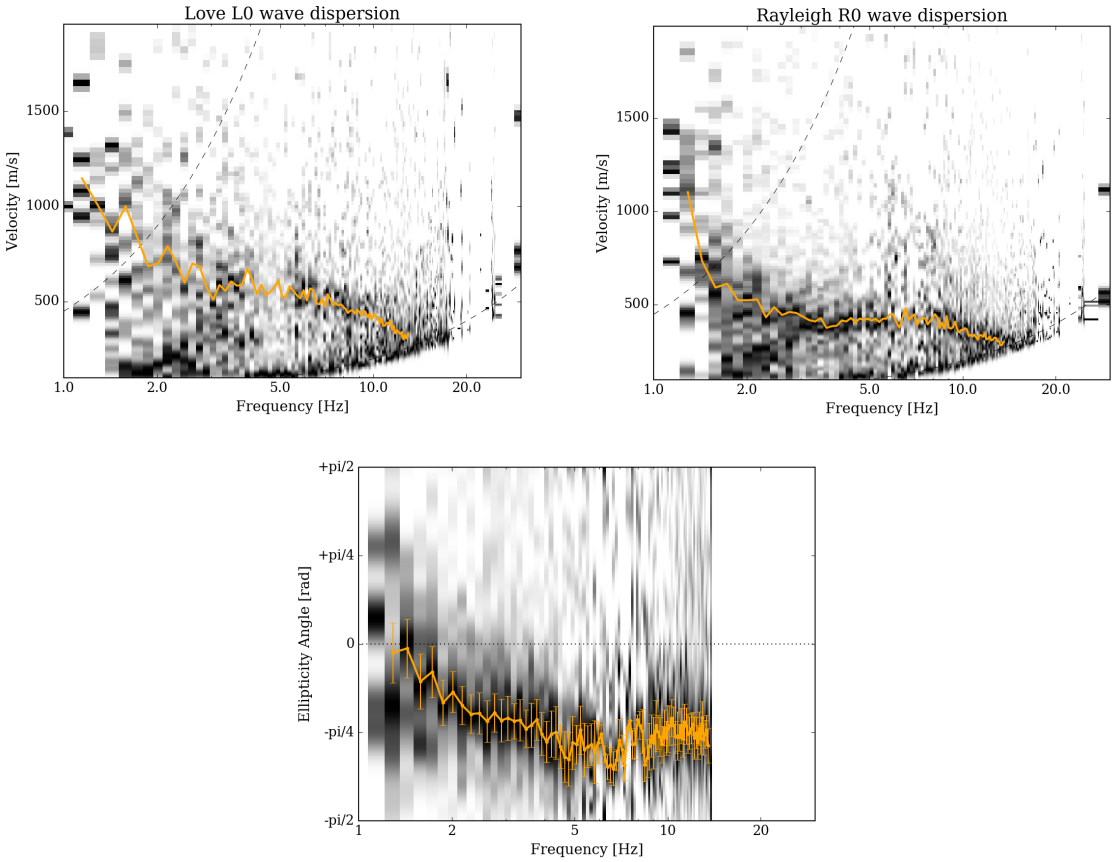

Figure 10: Dispersion curves for Love and Rayleigh waves (top row) and ellipticity angle curve for Rayleigh waves (bottom row) as obtained with WaveDec (Maranò et al., 2012). The dashed black lines (top rows) represent the array resolution limits, the solid orange line indicates the picked curve and the vertical bars at each frequency show the standard deviation for the ellipticity angle curves.

3.6 Modified SPatial AutoCorrelation

The SPAC (Aki, 1957) curves of the vertical components have been calculated using the MSPAC (Bettig et al., 2001) technique implemented in Geopsy (Wathelet et al., 2020). Rings with different radius ranges are defined and for all stations pairs with distances inside this radius range, the cross-correlation is calculated in different frequency ranges. These cross-correlation curves are averaged for all station pairs of the respective ring to give the SPAC curves. The rings are defined in such a way that at least three station pairs contribute and that their connecting vectors have a good directional coverage.

The SPAC Autocorrelation curves are shown in Fig. 11 for all selected rings (central and right columns). The black points indicate the data values which contributed to the final dispersion curve estimation, which was picked using the *spac2disp* function of the Geopsy. A single dispersion curve was picked for the Rayleigh wave between 0.95 and 10.70 Hz as shown by the gray curve

in Fig. 11 (left). The picked curve presents a long descending flank up to about 3 Hz followed by a flat portion.

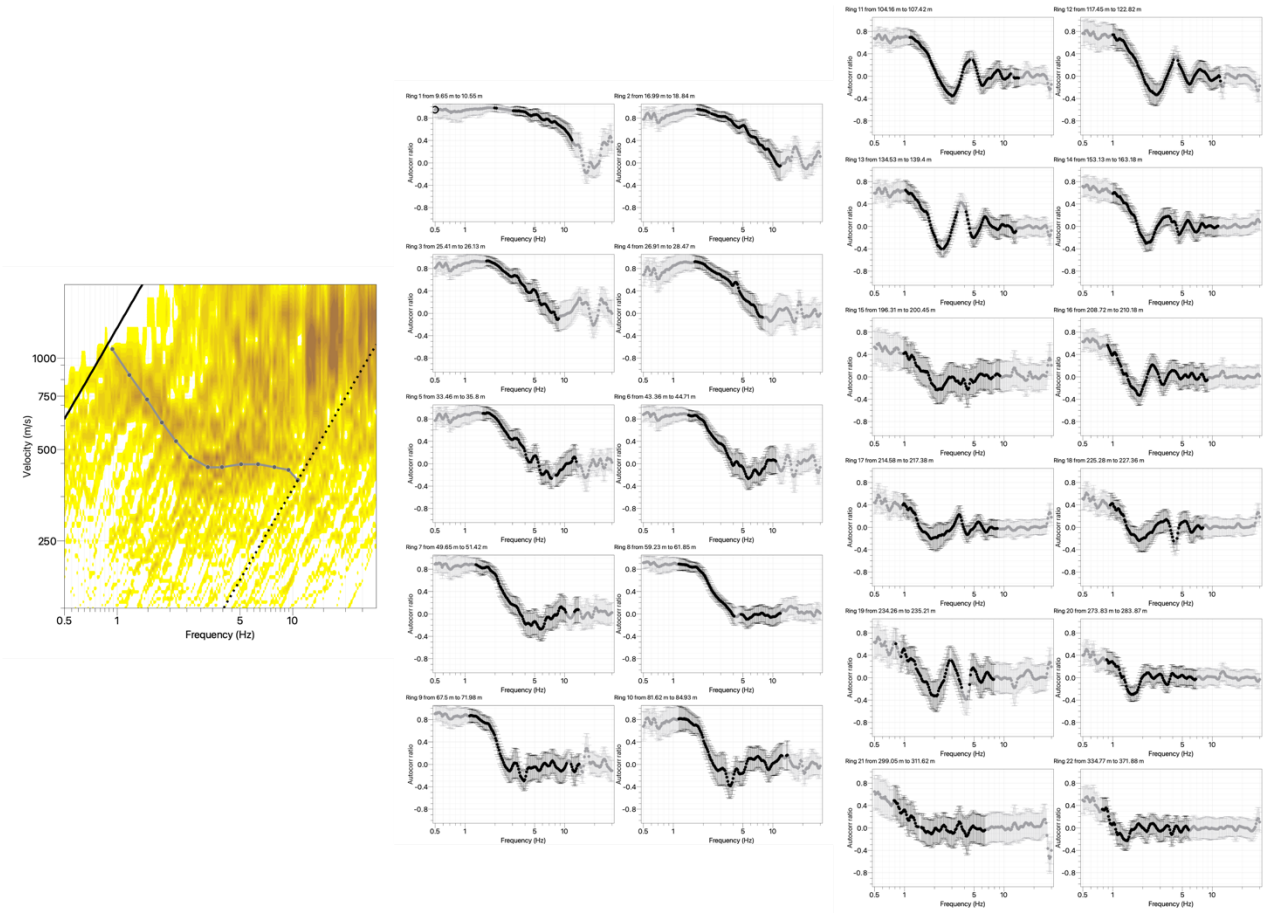

Figure 11: Rayleigh wave dispersion curve (left) obtained using spac2disp module of geopsy and autocorrelation functions for all rings (center and right). The solid gray line represents the picked data; the black dashed and dotted lines indicate the array resolution limits.

3.7 Summary

Figure 12 gives an overview of the Love and Rayleigh wave dispersion curves (left and central plots, respectively) and of the Rayleigh wave ellipticity curves (right plot) determined using different approaches. For Love waves, WaveDec and 3C-HRFK techniques produce one and two dispersion curves, respectively. The WaveDec curve and the curve at low velocity for the 3C-HRFK technique stretch over the frequency range 1.2 – 15.1 Hz. Their velocities are similar but some difference can be seen in terms of shape between 2 and 4 Hz. The curves picked using 3C-HRFK and WaveDec methods are interpreted as the fundamental mode of Love waves. The curve at higher velocities between 8.3 and 20.6 Hz and parallel to the other mode didn't received any mode attribution. For the Rayleigh waves, one curve was picked using WaveDec, one using MSPAC and four using the 3C-HRFK: two for the vertical component and two for the radial component. The WaveDec curve, the MSPAC curve and the two curves at low velocity for the vertical and radial components of 3C-HRFK perfectly overlap over the entire frequency range and

show a descending flank, a flat portion and a second descending portion. These curves are interpreted as the fundamental mode of Rayleigh waves. The two curves at higher velocity for the 3C-HRFK are straight and overlap between 5.5 and 14.5 Hz.
The ellipticity curves retrieved using the different methods are shown in the right plot of Fig. 12. The RayDec curves are shown for SSMS69 (dark green), the array center, and SSMS48 (light green), the closest station to SSMS station. The two curves show similar shapes but different amplitudes over the entire frequency range.
Four ellipticity curves were picked for the 3C-HRFK method: two for the vertical component and two for the radial component. These curves were picked over the same frequency range as the dispersion curves. The two ellipticity curves for the radial components are almost flat and shifted towards higher values when compared with the vertical curves. The mode at low velocity for the vertical component shows a wide trough, a wide and almost flat peak and a second trough, while the second mode has only a trough. The two ellipticity curves picked using the vertical component of 3C-HRFK show some similarities with the RayDec curve (SSMS69) above 3 Hz.
The ellipticity angle picked using the WaveDec technique is here shown as ellipticity curve. It goes from 1.29 to 13.53 Hz and fit perfectly the RayDec curve picked for SSMS69 above 1.8 Hz. The fundamental mode for the Rayleigh wave ellipticity curve is defined using the RayDec curve for station SSMS69 between 0.41–22.90 Hz.

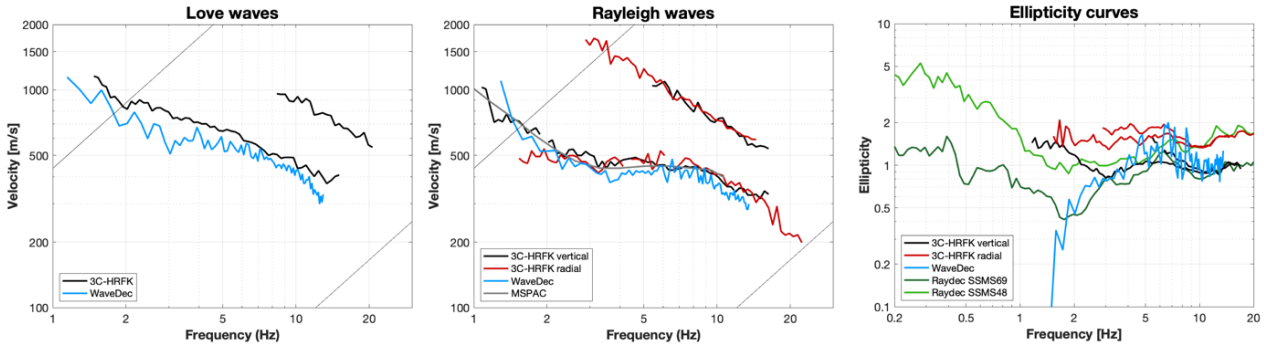

Figure 12: Comparison between the computed Love (left) and Rayleigh (center) wave dispersion curves and ellipticity curves (right).

4 Data inversion

4.1 Inversion targets

We performed four preliminary inversions combining the information of the picked dispersion and ellipticity angle curves. These tests were aimed at finding the correct mode attribution to the picked curves and perform the inversion using as much information as possible. The first inversion was performed using the dispersion curves only: one for the Rayleigh waves (1.08-16.30 Hz) and one for the Love waves (1.48-15.06 Hz). Both dispersion curves were interpreted as fundamental modes and were used in the same way in all four inversions. The other three inversions differ for the portion of ellipticity angle curve used. In the first case the ellipticity angle curve picked using WaveDec technique and with retrograde particle motion (1.47-13.2 Hz) is used. The second inversion combines two ellipticity angle curves, one with negative values (1.47-13.2 Hz) picked using WaveDec and one with positive values (0.36-0.92 Hz) identified using the 3C-HRFK technique. The last inversion uses the ellipticity curve computed using RayDec technique for the

array central station (SSMS69). The chosen ellipticity curve stretches over the frequency range 0.41-22.90 Hz and it is converted to ellipticity angle curve. Only the negative values are taken into account in the inversion. Of the four tested inversions, the last configuration is used and tested using five different parametrizations with an increasing number of layers. The details of the inversion targets are reported in Table 1 and the corresponding curves are shown in black solid lines in Fig. 13.
In the inversion process, we inverted two dispersion curves (Fig. 13 – left and center), one for the Love wave and one for the Rayleigh wave, and the Rayleigh wave ellipticity curve (Fig. 13 - right).

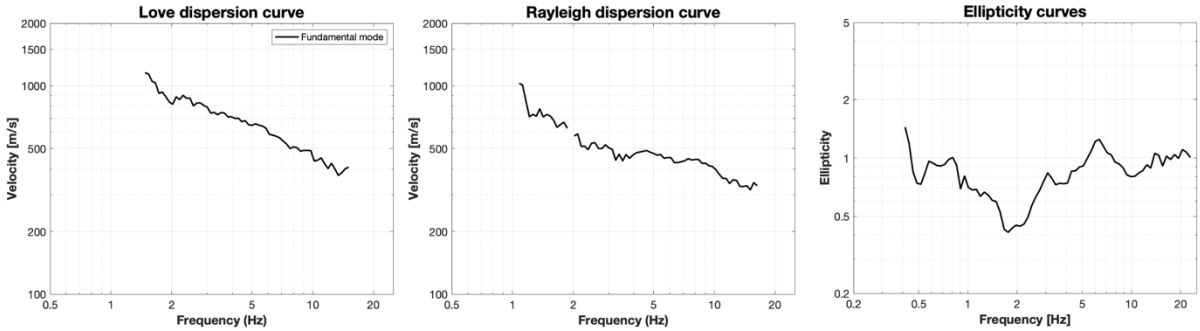

Figure 13: Overview of the dispersion curves used as target for the different inversions.

Table 1: List of the curves used as target in the inversion.

Method	Wave type	Mode	Curve type	Frequency range [Hz]
3C-HRFK	Love	fundamental	dispersion	1.48-15.06
3C-HRFK	Rayleigh	fundamental	dispersion	1.08-16.30
RayDec (SSMS69)	Rayleigh	fundamental	ellipticity	0.41–22.90

4.2 Inversion parameterization

For the inversion, five different parameterizations were tested. The first four involve free values of thickness and velocities for the different layers, ranging from six to twelve layers over the half-space. The S- and P-wave velocities are allowed to range from 50 to 3500 m/s and from 100 to 7500 m/s, respectively. The deepest interfaces were allowed to range to a depth of 750 m for all four parameterizations; the density was fixed to 2500 kg/m^3 for the bedrock layer and to 2000 kg/m^3 for all the other layers.
The last parametrization had fixed layer thicknesses and consists of 21 layers over the half-space, with the deepest interface at 700 m depth. Equal ranges were defined for the P- and S-wave velocities, while the density increases gradually from the twelfth layer (2000 kg/m^3) to the half-space (2500 kg/m^3).
In all parametrizations, velocity inversion was allowed for the shallowest layers down to a maximum depth of 100 meters.

4.3 Inversion results

We performed 5 inversions with different parameterizations (see Table 2) using the *dinver* routine (http://www.geopsy.org/). These present an increasing number of layers over the half-space ranging between 6 and 12. Each inversion run produced 280000 models to assure a good

convergence of the solution. The results of these inversions are shown in Figs. 14 – 18, while the minimum misfit out of the ten runs performed for each parametrization is reported in Table 2.

Table 2: List of inversions

Inversion	Number of layers	Number of models	Minimum misfit
SSMS 7l	7	280000	0.764
SSMS 9l	9	280000	0.512
SSMS 11l	11	280000	0.565
SSMS 13l	13	280000	0.625
SSMS fix	21	280000	0.698

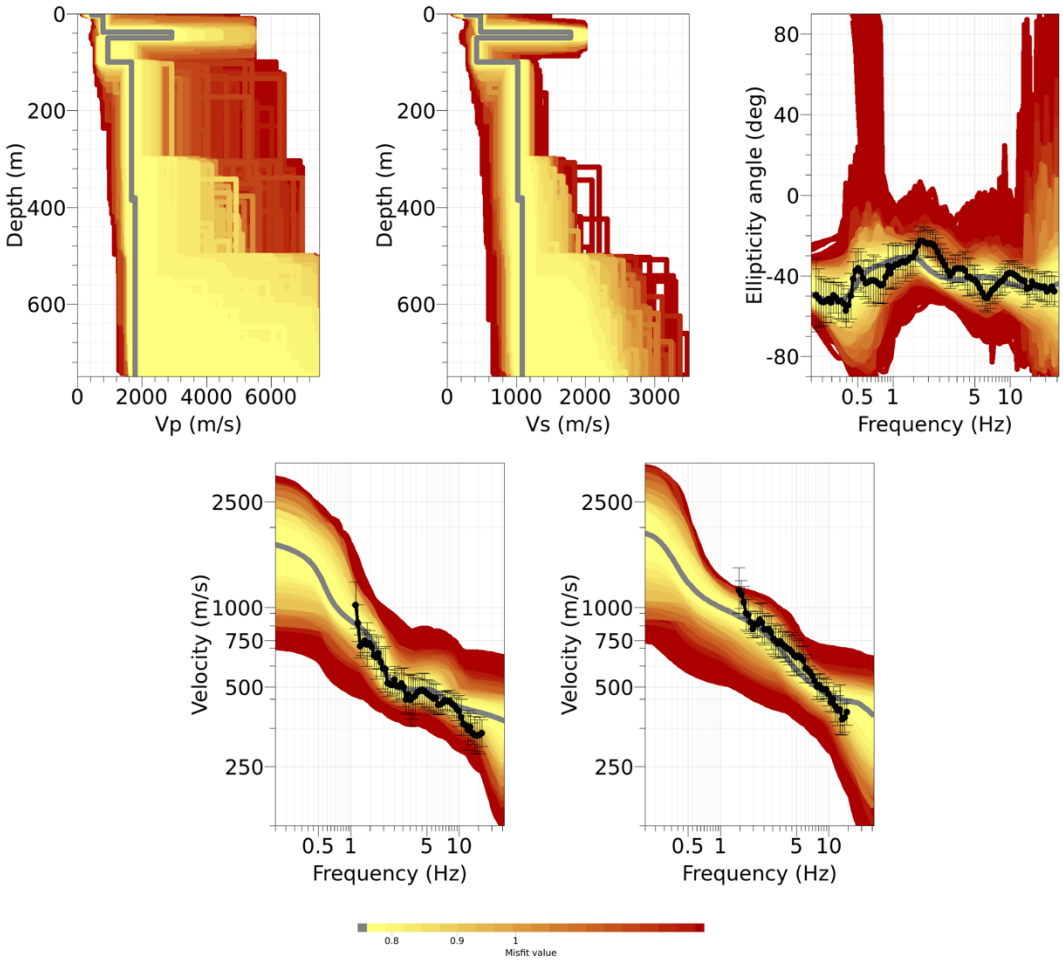

Figure 14: Inversion SSMS 7l. Top line: P-wave velocity profiles (left), S-wave velocity profiles (center) and Ellipticity angle curve (right). Bottom line: Dispersion curves for the fundamental mode of Rayleigh waves (left) and fundamental mode of Love waves (right). The black dots indicate the data points used for the inversion, the black bars the standard deviation of the inverted curve, while the gray line shows the best-fitting model.

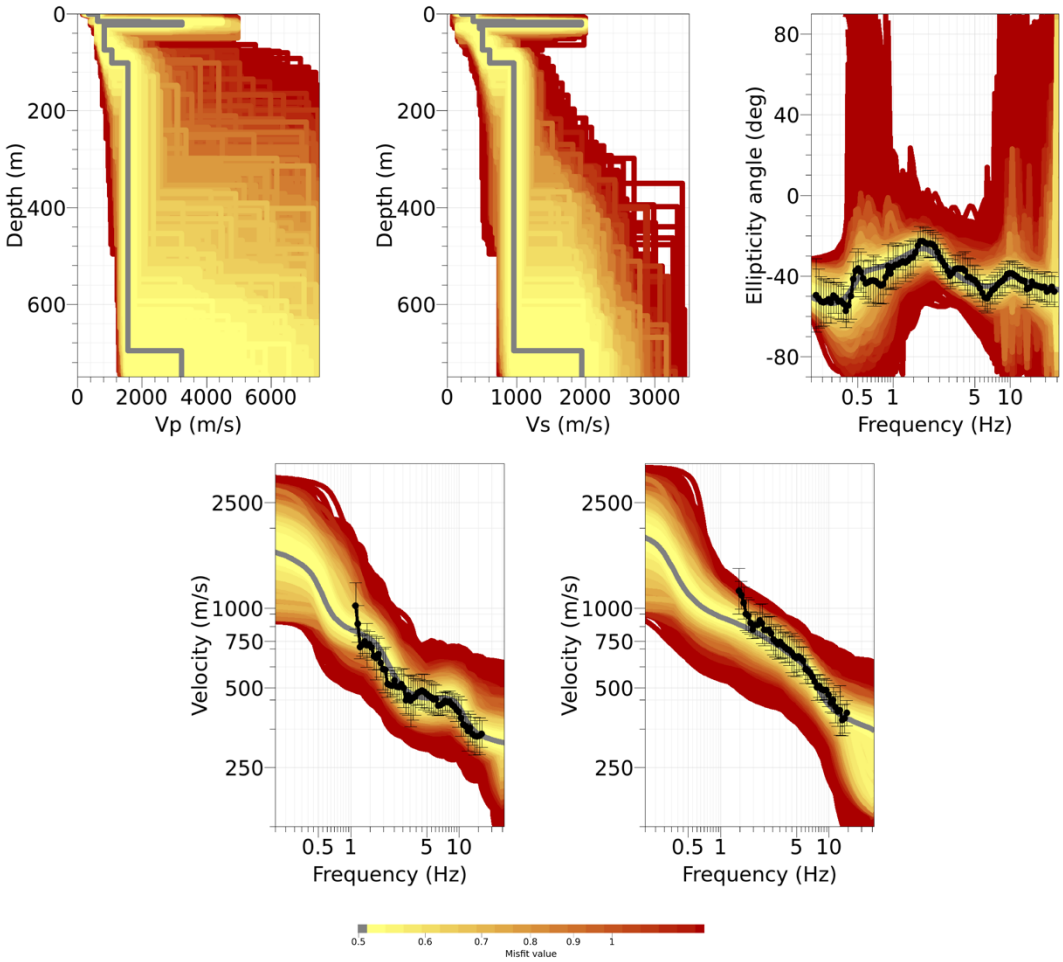

Figure 15: Inversion SSMS 9l. Top line: P-wave velocity profiles (left), S-wave velocity profiles (center) and Ellipticity angle curve (right). Bottom line: Dispersion curves for the fundamental mode of Rayleigh waves (left) and fundamental mode of Love waves (right). The black dots indicate the data points used for the inversion, the black bars the standard deviation of the inverted curve, while the gray line shows the best-fitting model.

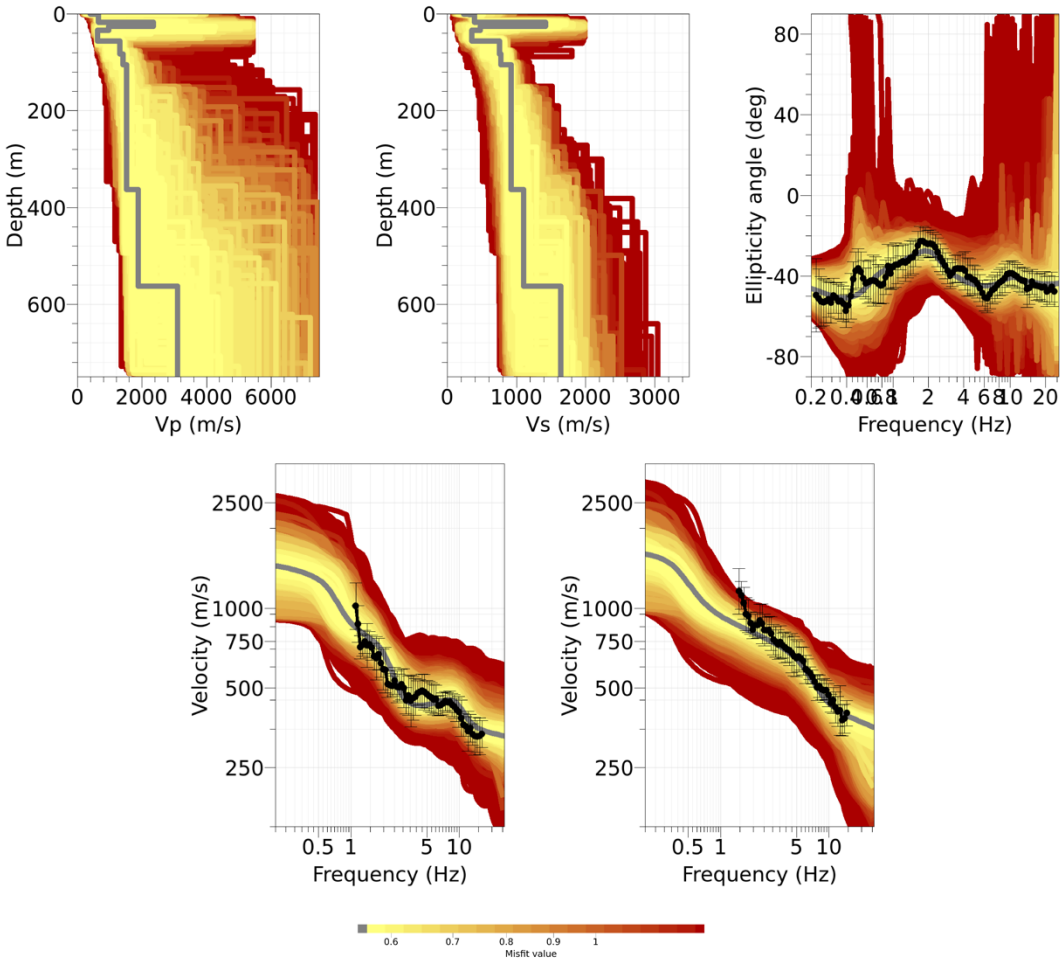

Figure 16: Inversion SSMS 11l. Top line: P-wave velocity profiles (left), S-wave velocity profiles (center) and Ellipticity angle curve (right). Bottom line: Dispersion curves for the fundamental mode of Rayleigh waves (left) and fundamental mode of Love waves (right). The black dots indicate the data points used for the inversion, the black bars the standard deviation of the inverted curve, while the gray line shows the best-fitting model.

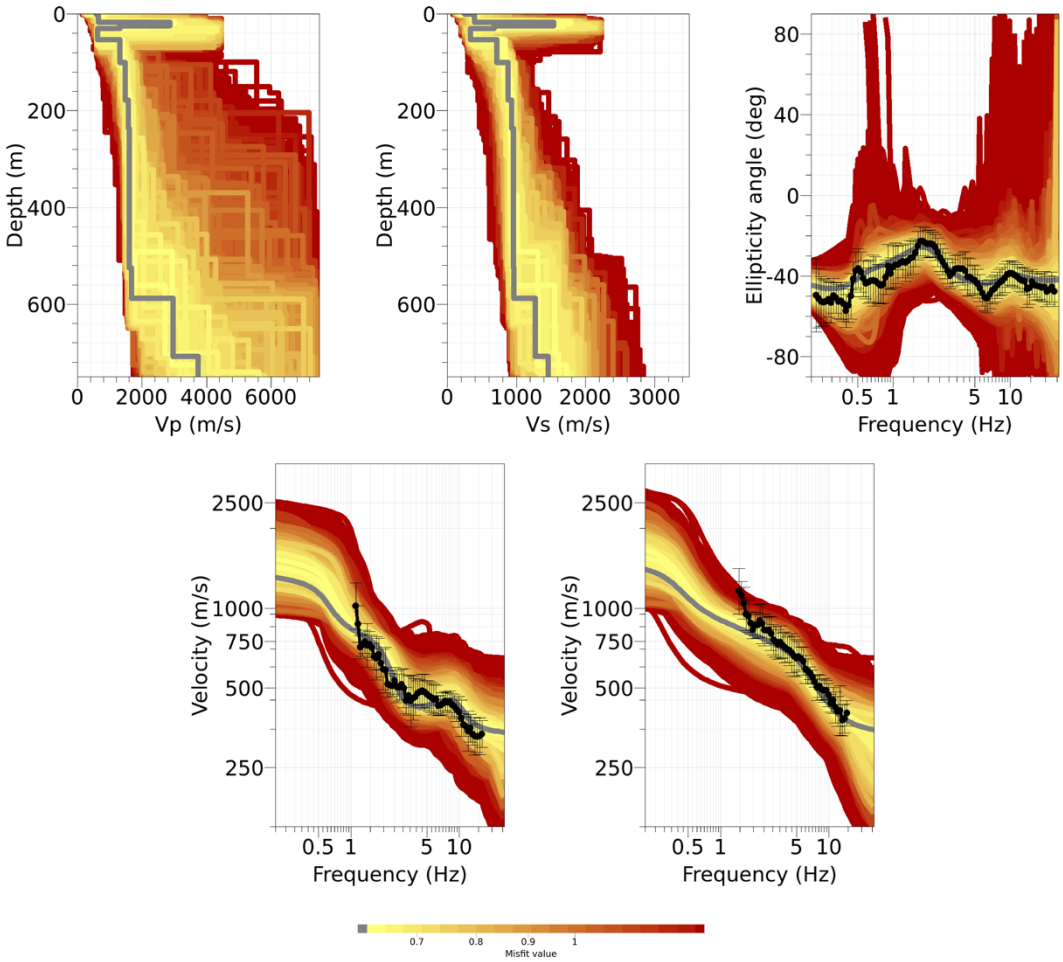

Figure 17: Inversion SSMS 13l. Top line: P-wave velocity profiles (left), S-wave velocity profiles (center) and Ellipticity angle curve (right). Bottom line: Dispersion curves for the fundamental mode of Rayleigh waves (left) and fundamental mode of Love waves (right). The black dots indicate the data points used for the inversion, the black bars the standard deviation of the inverted curve, while the gray line shows the best-fitting model.

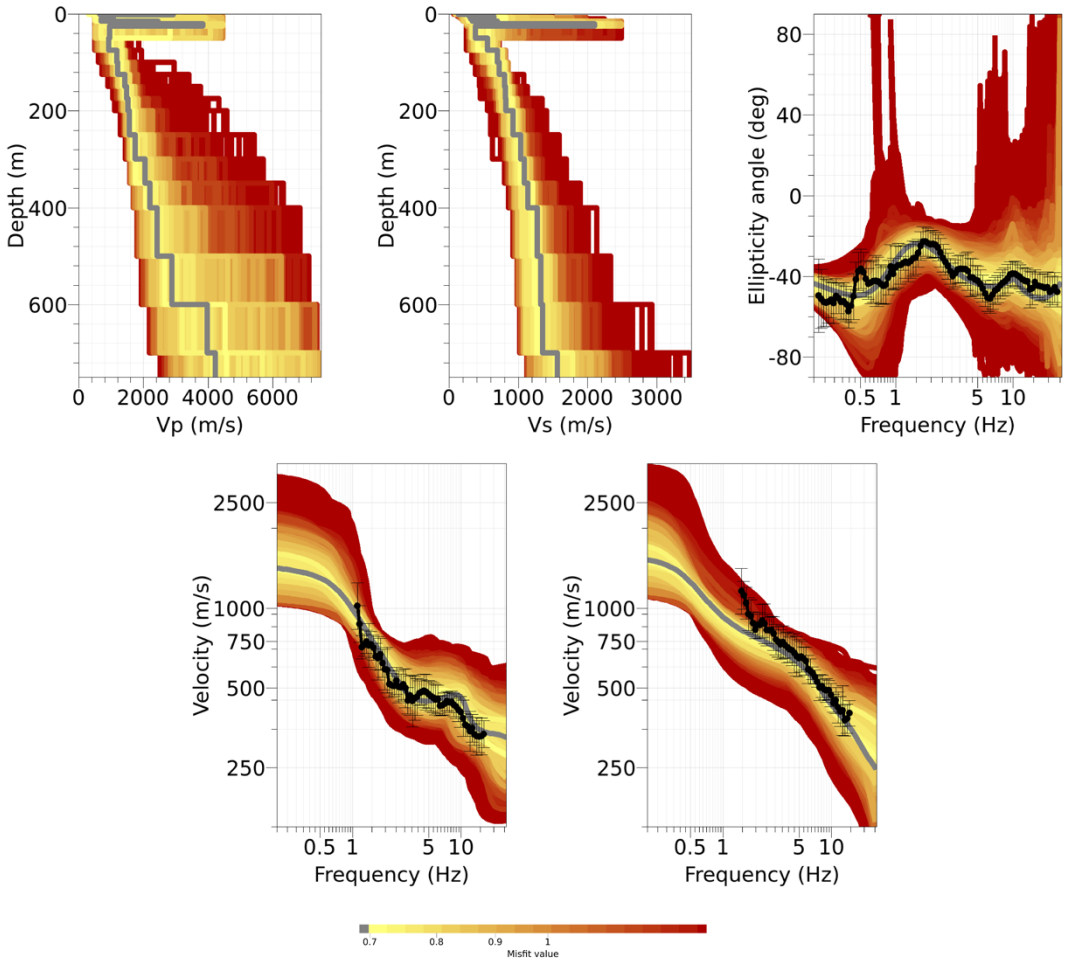

Figure 18: Inversion SSMS fix. Top line: P-wave velocity profiles (left), S-wave velocity profiles (center) and Ellipticity angle curve (right). Bottom line: Dispersion curves for the fundamental mode of Rayleigh waves (left) and fundamental mode of Love waves (right). The black dots indicate the data points used for the inversion, the black bars the standard deviation of the inverted curve, while the gray line shows the best-fitting model.

4.4 Inversion results - Neopsy

In addition to the five inversions performed using the *dinver* routine, the inversion is also performed using the multizonal transdimentional Bayesian formulation (Neopsy – Hallo et al. 2021). The targets of the inversion are the fundamental modes of Rayleigh and Love waves dispersion curves and the fundamental mode of Rayleigh wave ellipticity curve. The parametrizations for the seismic velocities, density, Poisson's ratio and depth are defined within ranges: the S- and P-wave seismic velocities range from 50 to 3500 m/s and from 100 to 7500 m/s, respectively; the density adjusts between 2000 and 3000 kg/m^3, while the Poisson's ratio is set to change between 0.2 and 0.45. The maximum depth is set to 800 m and the velocity inversion is allowed from the surface down to 100 meters. The inversion produced 5000 initial models and 25000 new models for a total of 30000 models.

The results of the inversion are shown in Figs. 19 and 20. Fig. 19 shows the fit of the measured curves used in input, while Fig. 20 displays the corresponding posterior marginal Probability Density Functions (PDF) and the resulting profiles for v_p, v_s, ρ and υ. The blue profile shows the best model using the Maximum Likelihood (ML), while the magenta color represents the model with the best Maximum A Posteriori (MAP) probability.

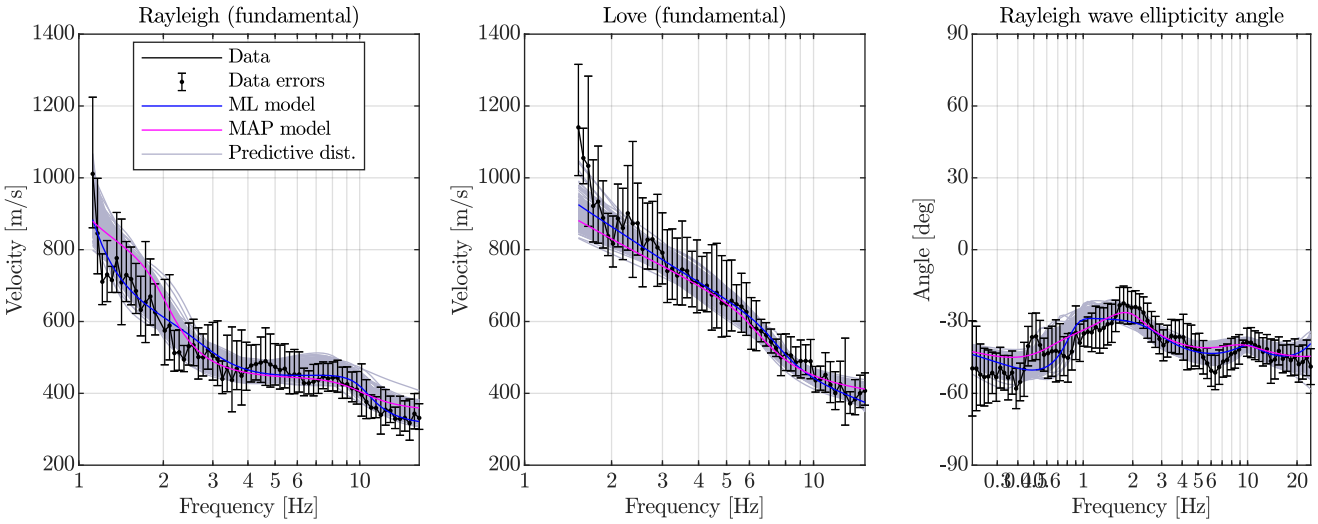

Figure 19: Results for the inversion using multizonal transdimensional Bayesian formulation. From left to right: Rayleigh waves fundamental mode, Love waves fundamental mode and Rayleigh wave ellipticity curve.

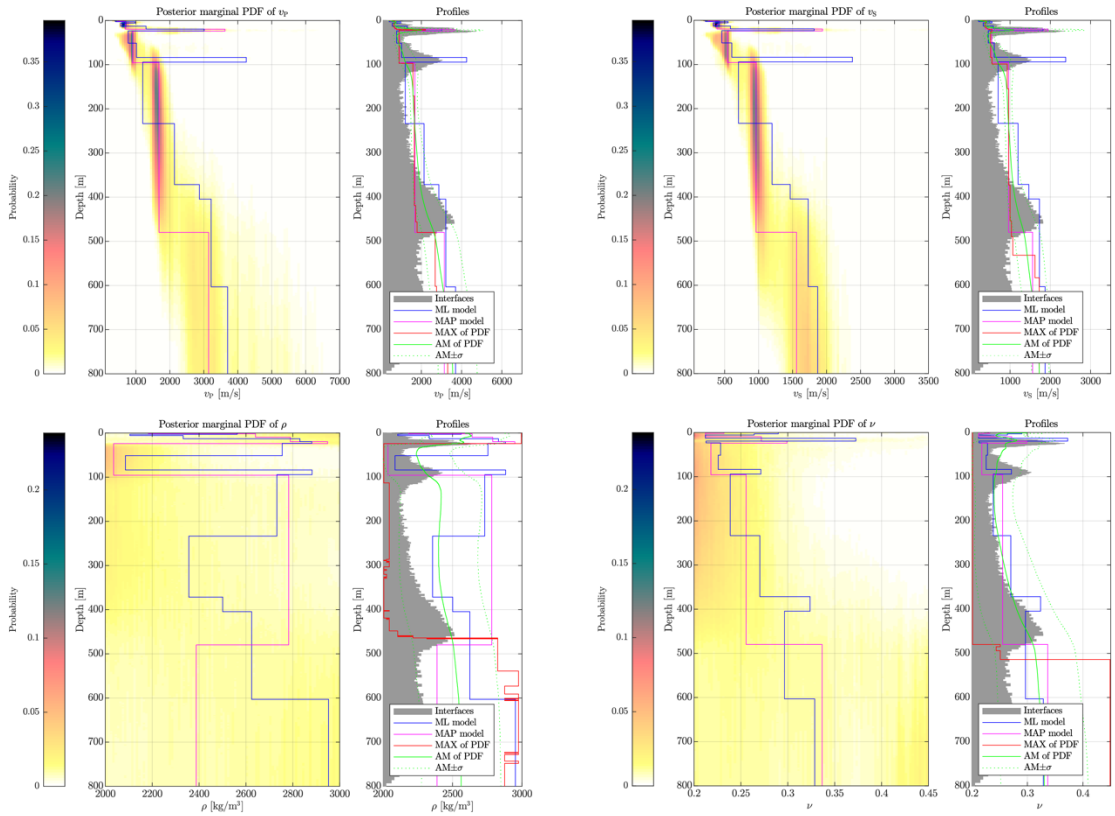

Figure 20: Posterior marginal PDF and profiles of P-waves (top left), S-waves (top right), density (bottom left) and Poisson's ratio (bottom right). Overview of the best profiles for each PDF for the Maximum Likelihood model (ML - blue) and the Maximum A Posteriori model (MAP - magenta).

4.5 Discussion of the inversion results

The models with the lowest misfit are shown in Fig. 21. The results of *dinver* inversions are shown in green and grey, while the models from *Neopsy* are displayed in blue and magenta and correspond to the best models from the Maximum Likelihood and Maximum A Posteriori models, respectively.

In the first 30 meters (Fig. 21 – right plot), all velocity profiles show a thin layer of 2-3 m with S-wave velocities of about 245 m/s followed by a second and thicker layer with an average S-wave velocity of about 400 m/s. Fix layers parametrization (*SSMS fix*) and Neopsy models, instead of showing a unique layer, present a weak velocity inversion down to 16 m. At about 17 m, a strong increase of S-wave velocity followed by a velocity inversion can be seen in all velocity profiles. This layer with S-wave velocities between 1425 and 2101 m/s has a thickness ranging between 4 and 9 meters. At about 101 meters, the *dinver* velocity profiles and the MAP model show a similar interface with S-wave velocities between 878.9 and 1019.2 m/s. The fix layer velocity profile in grey (*SSMS fix*) shows the same interface without any strong velocity contrast, as for the other profiles. The ML model, instead, presents a second strong velocity contrast with S-wave velocity up to 2380 m/s followed by a velocity inversion starting at 94 m and S-wave velocities of 703.8 m/s.

The depth of the half-space interface is not consistent among the inversions. The *dinver* velocity profiles in green and the MAP model show a strong velocity contrast at depths between 479.8 and 750 m. The fix depth layer (*SSMS fix*) shows a similar interface at 700 m with S-wave velocity of 1567 m/s. The ML model, instead, shows much lower or higher velocities when compared to the other velocity profiles. The half-space of the ML profile is at about 603 m and presents S-wave velocities of 1870 m/s.
The velocity profiles resulting from the different inversions have V_{S30} between 424.3 and 507.6 m/s, with an average value of 469.67 ± 32.97 m/s. The Vs30 for the MAP and ML models from Neopsy inversion are 462.33 and 443.82 m/s, respectively.

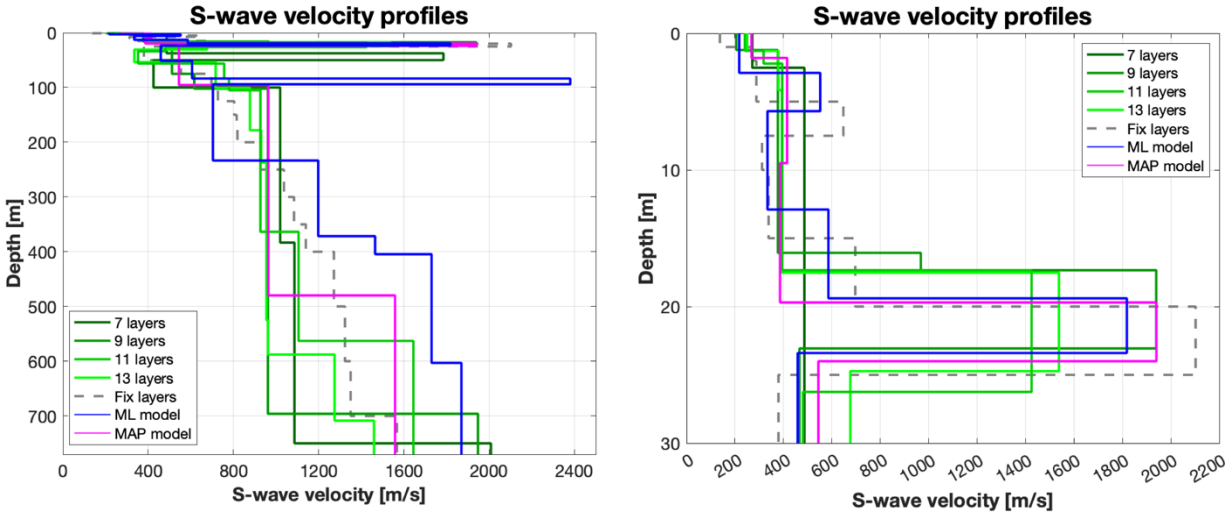

Figure 21: Overview of the best shear-wave velocity profiles of the different inversions (left) and zoom on the upper 30 m of the inversion profiles.

5 Further results from the inverted profiles

5.1 SH transfer function

The average theoretical shear-wave transfer functions for the best models of all tested parametrizations are shown in Figure 22. The SH-wave transfer functions for *dinver* (gray/black curve) and MAP (magenta) models are similar over the entire frequency. Their similarity can be appreciated in terms of shape and amplification values. The SH-wave amplification function for the ML model in blue presents numerous and sharp peaks with amplitudes between 3.5 and 13. Taking into account a smoothed version of the SH-wave function for the ML model we might recognized some similarity, in terms of shape and amplitude, with the two curves previously described.
The empirical amplification function (16.06.22) is presented in red in Fig. 22. It was obtained using a maximum number of earthquakes between 1.29 and 9.54 Hz, decreasing to 0 above 30.0 Hz. Above 1.8 Hz, the gray/black model and the MAP model have amplification values comparable with the empirical amplification function but different shape. At lower frequency, the empirical amplification function diverges towards lower amplifications. The discrepancy seen between the measured empirical amplification and the SH-wave transfer functions might be explained taking into account the distance between the center of the array and the location of SSMS

station (about 90 m) but also in terms of proximity of the permanent installation with the limestone cliff.

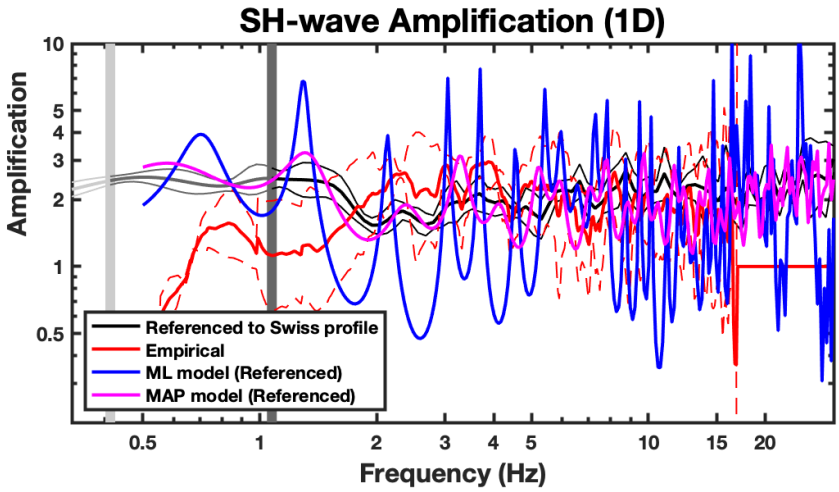

Figure 22: Modeled amplification function and standard deviation (black lines). Red curves represent the empirical amplification (solid line) and its standard deviation (dashed lines) function at the station SSMS.

5.2 Quarter-wavelength representation

The quarter-wavelength velocity approach (Joyner et al., 1981) provides, for a given frequency, the average velocity at a depth corresponding to 1/4 of the wavelength of interest. Figure 23 shows the quarter-wavelength results using the best models of Fig. 15 obtained inverting the fundamental modes of Rayleigh and Love wave dispersion curves together with the Rayleigh wave ellipticity angle for the fundamental mode. The results using this proxy, considering frequency limits of the experimental data between 1.1 to 16.3 Hz for the dispersion curves and between 0.4 and 22.9 Hz for the ellipticity curves, is well constrained down to 500 m. The quarter-wavelength impedance contrast introduced by Poggi et al. (2012) is also displayed in the Fig. 23. It corresponds to the ratio between two quarter-wavelength average velocities, respectively from the top and the bottom part of the velocity profile, at a given frequency.

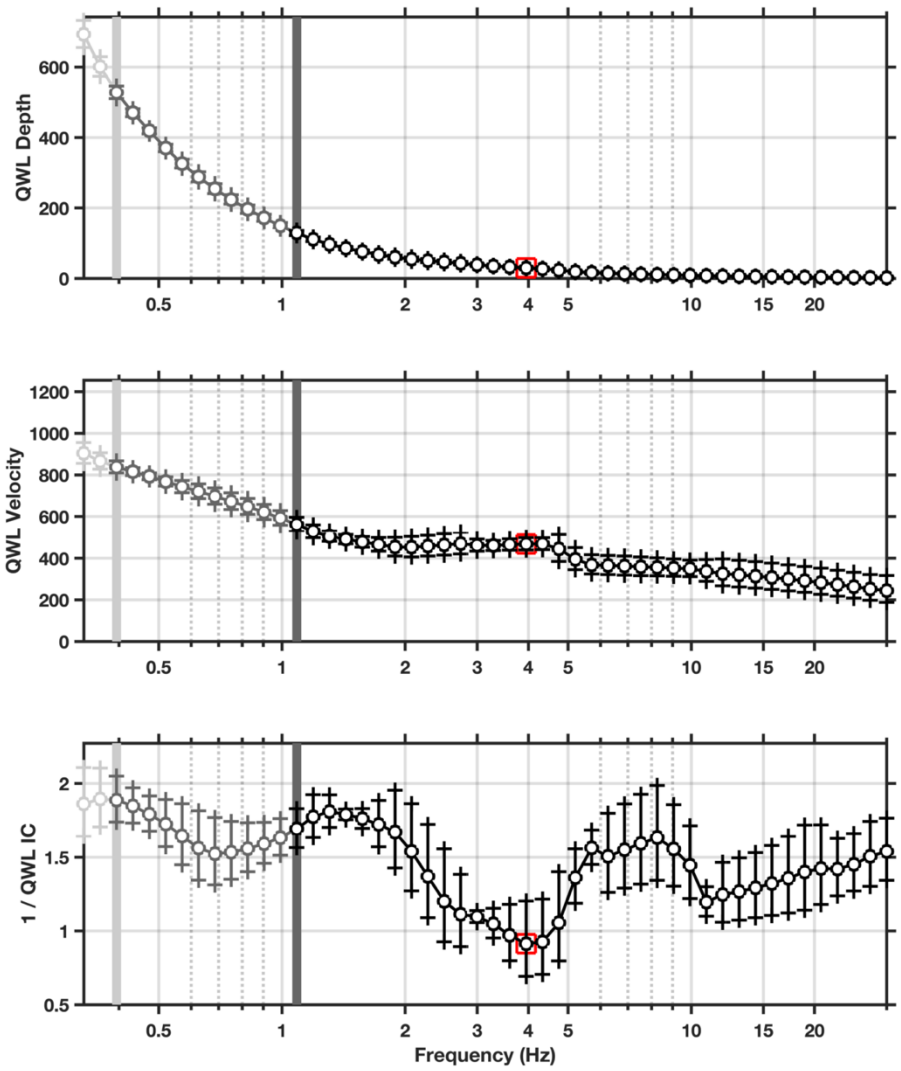

Figure 23: Quarter wavelength representation of the velocity profiles for the best models of the inversions (top: depth, center: velocity, bottom: impedance contrast). The grey light bar shows ellipticity lower frequency value, dark grey bar indicates lower frequency value obtained with dispersion curves and red square corresponds to f_{30} (frequency related to the depth of 30 m).

6 Discussion and conclusions

The passive array measurement performed in Saint Maurice in September 2021 allowed the investigation of the subsurface underneath the SSMS station.

The H/V analysis shows a homogeneous subsurface consisting in two main interfaces as shown by the two H/V peaks. The first one, at about 0.4 Hz, is visible only at the center of the deployed array; the second, much shallower, is picked over the entire study area between 4.87 and 7.74 Hz and shows a frequency variation moving from north to south. A third peak (at 0.7 Hz) was recognized at two sites using the information of the Fourier spectrum for the vertical component

and not the shape of the H/V curves. Curves with similar shapes and amplitudes were also computed using the RayDec technique (Fig. 5 – right plot).
The inversion of Rayleigh and Love wave dispersion curves and of the Rayleigh wave ellipticity angle curve yields to the estimation of P- and S-wave velocity profiles investigating the subsurface down to about 770 m. All velocity profiles show one interface at about 2-3 m and a second one at about 17 m followed by a strong velocity contrast and a velocity inversion. At about 100 m a third interface can be seen by most of the velocity profiles. The depth and the S-wave velocity of the half-space is not consistent among the inverted velocity profiles. It is located between 495 and 750 meters by most of the models and has S-wave velocities between 1460 and 2008 m/s.
The V_{S30} value of the site is 495.1 m/s, corresponding to soil class B in EC8 and C in SIA261.
The theoretical shear-wave transfer functions for the *dinver* velocity profiles and the MAP model predict a rather flat amplification with wide and small peaks at about 1.3, 8 and 17 Hz. The comparison with the SSMS empirical amplification function shows similar amplification values above 2 Hz but different shapes. At lower frequency, the empirical curve diverges towards lower values. The SH-wave transfer function for the ML model consists in narrow and sharp peaks not fitting the empirical amplification; a smoothed version of this curve might help to find similarities with the SH-wave amplification for the MAP model.

References

Burjánek, J., Gassner-Stamm, G., Poggi, V., Moore, J. R., and Fäh, D. (2010). Ambient vibration analysis of an unstable mountain slope. Geophys. J. Int., 180:820–828.

Burjánek, J., Moore, J. R., Molina, F. X. Y., and Fäh, D. (2012). Instrumental evidence of normal mode rock slope vibration. Geophys. J. Int., 188:559–569.

Fäh, D., Gardini, D., et al. (2003). Earthquake Cataloque of Switzerland (ECOS) and the related macroseismic database. Eclogae geol. Helv. 96.

Fäh, D., Wathelet, M., Kristekova, M., Havenith, H., Endrun, B., Stamm, G., Poggi, V., Burjanek, J., and Cornou, C. (2009). Using ellipticity information for site characterisation. NERIES deliverable JRA4 D4, available at http://www.neries-eu.org.

Fritsche, S., Fäh, D., Gisler, M., and Giardini, D. (2006). Reconstructing the damage field of the 1855 earthquake in Switzerland: historical investigations on a well-documented event Geophys. J. Int., 166, 719–731

Hallo, M., Imperatori W., Panzera F. and Fäh, D. (2021). Joint multizonal transdimensional Bayesian inversion of surface wave dispersion and ellipticity curves for local near-surface imaging. Geophys. J. Int., 226, Issue 1, 627-659

Hobiger, M., Bard, P.-Y., Cornou, C., and Le Bihan, N. (2009). Single station determination of Rayleigh wave ellipticity by using the random decrement technique (RayDec). Geophys. Res. Lett., 36.

Maranò, S., Reller, C., Loeliger, H.-A., and Fäh, D. (2012). Seismic waves estimation and wavefield decomposition: Application to ambient vibrations. Geophys. J. Int., 191:175–188.

Poggi, V. and Fäh, D. (2010). Estimating Rayleigh wave particle motion from three component array analysis of ambient vibrations. Geophys. J. Int., 180:251–267.

Poggi, V., Edwards, B., and Fäh, D. (2010). Characterizing the Vertical-to-Horizontal Ratio of Ground Motion at Soft-Sediment Sites. Bulletin of the Seismological Society of America, 102(6): 2741 2756.

Wathelet, M., Chatelain, L., Cornou, C., Giulio, G. D., Guillier, B., Ohrnberger, M., and Savvaidis, A., 2020. Geopsy: A User-Friendly Open-Source Tool Set for Ambient Vibration Processing, Seismological Research Letters, XX, 1–12.